Development of the Mod II X-57 Piloted Simulator and Flying Qualities Predictions

Ryan Wallace[1], James Reynolds[2], and Mike Frederick[3]
NASA Armstrong Flight Research Center, Edwards, California, 93523, USA

Dana Mcminn[4], Dave Cox[5], and Nick Borer[6]
NASA Langley Research Center, Hampton, Virginia, 23681, USA

This paper discusses the development of the X-57 Mod II piloted simulator along with the predicted flight dynamics of the airplane. The piloted simulator models were initially based on data published by Tecnam on a P2006T airplane but were further improved upon through parameter identification of flight data as well as modeling tools such as computational fluid dynamics. In addition to having accurate flight models, a realistic cockpit was constructed to aid pilot training. From the piloted simulator, an understanding of how the airplane will behave throughout the flight envelope using established FAR and MIL standards is discussed. Using the simulation results, this paper will show that the airplane is predicted to be statically and dynamically stable as well as having Level 1 flying qualities.

I. Nomenclature

C_L	= lift coefficient
$C_{L\alpha}$	= lift coefficient as a function of angle of attack
C_M	= pitching moment coefficient
deg	= degree
Fs	= stick force
g	= gravity
H_{MSL}	= altitude (measured sea level)
Kpo	= overspeed gain
Kpu	= underspeed gain
kts	= knots
Nm	= Newton-meters
p	= roll rate
q	= pitch rate
r	= yaw rate
RPM_{OUT}	= revolutions per minute output, used in fig 2
s	= seconds
$Torq_{Cmd}$	= commanded torque lever position
$Torq_{increase}$	= amount of torque added
$Torq_{out}$	= motor generated torque
$Torq_{reduce}$	= amount of torque reduced
V_{EAS}	= equivalent airspeed

[1] Aerospace Engineer, Flight Dynamics and Control Branch, AIAA Senior Member.
2 Aerospace Engineer, Flight Dynamics and Control Branch, nonmember.
3 Aerospace Engineer, Aerodynamic and Propulsion Branch, nonmember.
4 Aerospace Engineer, Dynamic Systems and Control Branch, AIAA Member.
5 Aerospace Engineer, Dynamic Systems and Control Branch, AIAA Senior Member.
6 Aerospace Engineer, Aeronautics Systems Analysis Branch, AIAA Associate Fellow.

V_T = true airspeed
$Vs1$ = takeoff configuration stall speed
$Vs0$ = landing configuration stall speed
n/α = Load factor as a function of angle of attack
CG = center of gravity
α = angle of attack
δa = aileron deflection
δe = elevator deflection
δr = rudder deflection
β = sideslip angle
ζ = damping ratio
Φ = roll angle
Ω = motor speed
$\Omega high$ = upper motor speed limit
Ωlow = lower motor speed limit
τ_r = roll mode time constant
ω = frequency
ω_{SP} = short-period frequency
ζ_{Ph} = phugoid damping ratio
ζ_{SP} = short-period damping ratio
ζ_{DR} = Dutch roll damping ratio

II. Introduction

Recent advances in battery technology have allowed for the ability to electrify aircraft. Because of these advances, small to large companies are evaluating the benefits of producing electric aircraft for the commercial market [1].

The National Aeronautics and Space Administration (NASA) X-57 ("Maxwell") project was developed to demonstrate distributed electric propulsion (DEP) for a general aviation airplane. A spiral developmental approach was taken by the project; three distinct phases (called "Mods") were intended to progressively add capability to the propulsion of the airplane and its electrical system as well as alter the wing planform, as described in Borer et al., [2]. This paper focuses on the "Mod II" of the project, as described below.

The Mod II X-57 airplane is a stock Tecnam (Costruzioni Aeronautiche Tecnam srl) (Capua, Italy) P2006T twin-engine airplane that was modified to replace the twin-100-horsepower Rotax (BRP-Rotax GmbH & Co KG) (Gunskirchen, Austria) 912S internal combustion engines with two JM-57 motors constructed by Joby Aviation (Joby Aviation, Inc.) (Santa Cruz, California). With the change from gas powered engines to electric motors, the spin direction of the left motor was switched from clockwise to counterclockwise resulting in counter rotating propellers; thus, minimizing out the P-factor. With the removal of the internal combustion engines, the P2006T fuel system was also removed from the airplane.

To power the Mod II motors, two lithium-ion battery packs developed by Electric Power Systems (Electric Power Systems LLC) (City of Industry, California) were installed in the fuselage section. Additional hardware such as a battery monitoring system, electrical cabling, and motor controllers were added to the airplane to support the electronification of the airplane. Further details of the Mod II electrical architecture are described in Clarke, et al., [3]. Since the airplane is a research vehicle, the project added sensor instrumentation with an onboard data recording system. A flight-test nose boom of the National Advisory Committee for Aeronautics (NACA) style was also added to the airplane to measure airspeed by capturing total pressure; static pressure; angle of attack (α); and sideslip angle (β).

The modifications to the P2006T airplane resulted in a shifted Center of Gravity (CG) location in all three axes, an increased total weight, and a change to the moment of inertias. The CG shift in the longitudinal direction remained within the P2006T Pilot Operation Handbook (POH) [4] limits but was further aft by 1.8 inches as compared to an empty stock P2006T airplane. In the vertical direction the CG was shifted 8.7-in downward, while the lateral direction CG was shifted 0.53-in left of the centerline. Compared to the empty stock P2006T airplane, the weight of Mod II had an increase of 212.5 pounds. An outcome of having an electric-powered aircraft is that the weight and CG locations remain constant throughout the flight; thus, there is an assumption that there will not be any changes to the flying qualities of the aircraft due to consumption of battery power throughout the length of the flight.

To prepare for the Mod II X-57 flights, a full nonlinear, piloted simulator was developed for pilot training and prediction of the flying qualities of the airplane. This paper describes the piloted simulator development and the predicted airplane flying qualities for the X-57 Mod II airplane.

III. Piloted Simulator Development

An initial X-57 simulator was developed using the commercial software, MATLAB R2016b and Simulink R2016b [5] and integrating together the aerodynamic, propulsion system, landing gear, atmospheric, mass properties, and actuator models. This simulator was primarily utilized for model development and batch analysis. A pilot-in-the-loop simulator was then developed by integrating an Autocoded C++ version of the Simulink models into the NASA Armstrong Flight Research Center (AFRC) (Edwards, California) Coresim Version 7 simulation architecture software [6]. A simulator X-57 cockpit that mimicked the layout of the airplane was constructed to interact with the simulation models.

A. Model Development

Aerodynamic Model

Overall, the airplane modifications as described in Section II to the P2006T Outer Mold Line (OML) were minor and were not expected to have significant effects on the aerodynamics of the airplane; therefore, the aerodynamic model for the Mod II airplane was based heavily on Tecnam P2006T data.

The initial Mod II aerodynamic-coefficient model was based on the published flight results from a Tecnam P2006T airplane [7]. Further development of the aerodynamic model utilized results from test flights conducted by NASA AFRC of an instrumented P2006T airplane. Data from the instrumented P2006T airplane such as inertial measurements, angle of attack, sideslip angle, and airspeed were used along with control surface deflections to perform parameter identification (PID) analysis. The PID analysis yielded aerodynamic coefficients as well as functions for multiple flight conditions and flap settings. Additional refinement on the lift coefficient as a function of angle of attack ($C_{L\alpha}$) was done by running the OML of the wing through a nonlinear lifting-line analysis that resulted in a curve that matched better to the Mod II flight data. Since the OML of the Mod II model closely matches that of the P2006T airplane, it is assumed that the stall characteristics are also similar. Stall is not modeled in the aerodynamic model, instead, to alert the pilot that the airplane is approaching stall, the simulator has an audio-stall warning system similar to the P2006T airplane audio-stall warning system. Ground effects were also not included into the model due to the assumptions that there would be a minimum effect on the high wing, and the planned takeoff speed of 1.2·Vs1 would provide ample margin above stall.

The airplane drag was modeled with the landing gear and flaps not deployed, which was derived from the performance tables in the P2006T POH. Flaps and landing gear drag increments (derived from the P2006T flight PID glide test points) were then added onto the clean airplane. The model also captured the moment effect from the contributions of the landing gear drag and moment arm on the airplane.

Additionally, the longitudinal stick forces were calculated using the airplane yoke moment arm, control surface position, airspeed, and hinge moments. The hinge moments lookup tables of the model were developed from computational fluid dynamics (CFD) analysis of the P2006T tail at three flap positions: 0, 10, and 30 degrees.

Based on the assumption that aerodynamics of the Mod II airplane are not too different from the P2006T airplane, the control surface inputs and flight conditions from the P2006T instrumented flights were inserted into the simulator for a comparison. A comparison between the P2006T flight and a simulation run is shown in Fig. 1; the figure shows a close match between the flight data and simulation data, indicating that the aerodynamic model matches the P2006T aerodynamics closely.

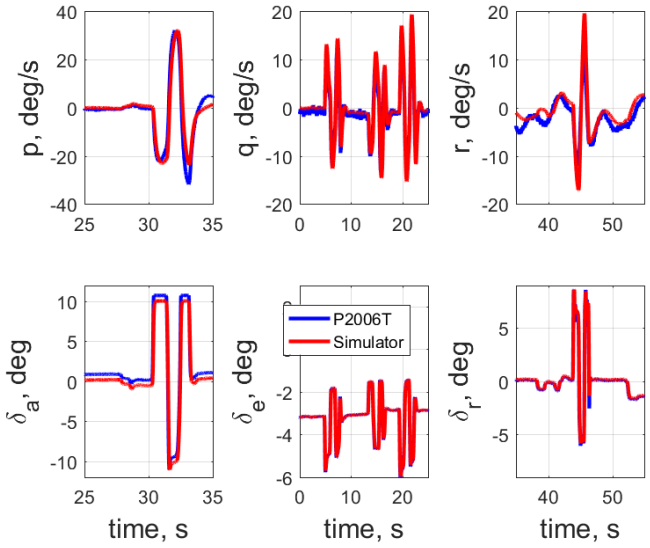

Fig. 1 P2006T flight data and simulator data comparison.

Propulsion Model

The electric motors are modeled as a proportional torque-to-motor-shaft power output system. Each motor is modeled with two cruise motor controllers (CMCs) supplying power; thus, the propulsion model has four CMCs to control the two motors. One CMC provides half the power to a motor, as described in Clarke et al., [3]. To replicate motor system power losses, a motor efficiency lookup table is applied to the current draw of the motor. Figure 2 shows data from initial ground testing of the motors and a simulator test at the same conditions. The tests swept through a torque command range at a constant revolutions per minute (RPM) command. From initial airplane motor testing, Fig. 2 shows that the ground test; simulator RPM output (middle graph); and estimated motor torque output (bottom graph) match well. The match between the motor ground testing and the simulation testing provides confidence that the propulsion model has the correct relationship between command input and motor output. The large ground test spikes in the RPM panel are due to data dropout during the run.

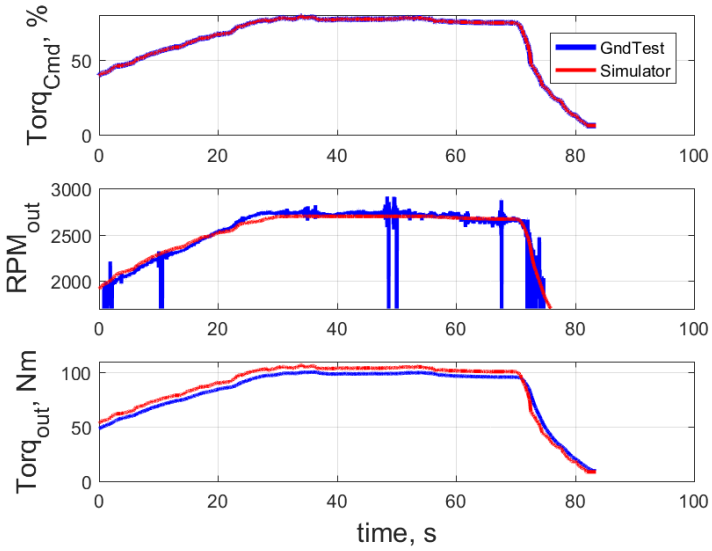

Fig. 2 Time history comparison of torque lever command, revolutions per minute output and estimated motor torque.

Torque command had three distinct mapping regions: regeneration, nominal, and overdrive. The regeneration region (-27 to -0.7-percent lever position) commands a negative torque to the motors which drives the propellers towards windmilling, which increases the drag torque on the motors. The nominal region (-0.7 to 100-percent lever position) commands a positive torque to the motors. At 100-percent torque lever position and 2700 RPM, both motors were designed to produce 255 Nm of torque. Within the nominal region there is a small idle region (-0.7 to 6.3-percent lever position) that commands 8 Nm of torque per motor controller, where the motors produce little to no thrust but still rotate. For additional power, the overdrive region (100 to 166-percent lever position) is capable of producing 175 Nm of torque per CMC. The overdrive region was designed for use with only one operating CMC per motor since the motor was designed for 255 Nm of torque.

The CMCs employ overspeed and underspeed protections that use a conditional torque weight represented by Eq. 1 and 2:

$$Torq_{reduce} = K_{po}\left(\Omega - \Omega_{high}\right)^2 \tag{1}$$

$$Torq_{increase} = K_{pu}(\Omega - \Omega_{low})^2 \tag{2}$$

Where K_{po} is the overspeed protection gain; K_{pu} is the underspeed protection gain; $(\Omega - \Omega_{high})$ is the difference between the motor speed and the upper motor speed limit; and $(\Omega - \Omega_{low})$ is the difference between the motor speed and the lower motor speed limit. If the RPM is above the motor speed of 2750, the overspeed protection subtracts a torque value calculated from Eq. (1) that reduces the motor speed. If the RPM is below 1100, the underspeed protection adds a torque value calculated from Eq. (2) that increases the motor speed. Included with the CMC modeling is a nominal efficiency of 97 percent, which represents a simplified and conservative value for losses within the controller itself.

The electric propeller hubs are a constant speed propeller system based on the electric variable-pitch propeller of the airplane, manufactured by MT-Propeller (MT-Propeller Gerd Muehlbauer GmbH) (Airport Straubing-Wallmeuhle, Germany) [8]. The propeller hubs are modeled as a rate-limited system in a servo loop which adjusts the pitch angle of the blades based on the commanded RPM and airspeed. The primary thrust and drag predictions are derived from the blade element predictions obtained by the open-source software, XROTOR (open-source software, Massachusetts Institute of Technology, Cambridge, Massachusetts) [9]. The CFD analysis was done to determine the off-axis inflow angles and steady-state windmilling drag data. Propeller inertial response to motor torque as well as propeller inertial coupling due to airplane rates are captured within the model.

The battery model is a Thevenin equivalent circuit model, based on the mission planning tool (MPT) developed by Chin et al., [10]. The Mod II simulator model uses motor efficiency, air data, airplane state, motor and propeller states, and control settings to produce an estimated battery state of charge (SoC) and battery temperature.

Landing Gear Model

The X-57 landing gear model was adapted from a legacy NASA Langley Research Center (LRC) (Hampton, Virginia) landing gear model which provided a generic architecture for nosewheel steering, tire traction, tire drag, strut dynamics, and wheel braking. A linear compression spring-damper post with a compressible tire was used to represent the nose gear, while the main gear was modeled as trailing arms with a spring-damper system and compressible tires.

The vertical forces of the gear were determined by the amount of spring compression and the rate of damper displacement. For each gear, the undeflected tire/gear ground contact point relative to the CG of the airplane was tracked. Upon landing touchdown, the distance of tire below the ground plane was calculated to be the tire compression which then was calculated to be the tire reaction force and translated into the vertical gear compression. Lateral gear forces were calculated from the vertical loads and scrub radius. Longitudinal gear forces were generated from both tire friction and braking. Tire friction was a function of the vertical loads upon the gear multiplied by the tire friction coefficient. Braking force would increase the tire friction coefficient by using a slip parameter as an input to a generic friction coefficient curve, which would then set the level of additional friction force upon the wheels. Increased braking caused increased tire friction and slip value, up to a point where skidding would occur, causing a loss in tire friction as the wheels locked up.

Mass Model

Aircraft component weights, moments of inertias, and CG location of the X-57 airplane are tracked in a detailed Computer Aided Design (CAD) model. The airplane properties in the CAD model are then integrated into the simulation mass model. An overall measurement of the weight (w) of the X-57 airplane and the longitudinal and lateral CG is provided through a weight-on-wheels measurement that is used as a validation of the CAD model mass

properties. The airplane has an overall weight of 2835.5 pounds, a longitudinal CG of 24.4 percent of the mean aerodynamic cord, and lateral CG of 0.53-in left of the airplane centerline. The predicted vertical CG is 22.7-in below the leading edge of the wing and moments of inertias (Ixx, Iyy, Izz) (or 6.29101e6, 8.51692e6, 1.30684e7 $lb{\cdot}in^2$, respectively).

B. Simulator Cockpit Development

A critical component of realistic-as-possible pilot training is having a simulator cockpit that represents the actual airplane cockpit. The simulator cockpit features items such as a dashboard (for the gauges and switches); control inceptors with a force feedback feel system; and a pilot seat, as shown in Fig. 3.

Fig. 3 Piloted simulator cockpit. Pilot seat, controls, switches, out-the-window view, and instrumentation.

Figure 4 shows the airplane dashboard is replicated in the piloted simulator by using a head-down display (HDD). The HDD of the simulator utilizes two touch screens to emulate the physical gauges on both the left and right dashboard panels found on the airplane, as shown in Fig. 5. The left-hand panel of the HDD contains the stock P2006T instruments in addition to an accelerometer (G-meter) and modified annunciator panel; the opposite side of the HDD (right-hand panel) displays the four-traction bus power meters, voltage-current DC converter meters, and two propellor tachometers. In the center of the simulator dashboard is a controller area network (CAN) bus reader called the multifunction display (MFD), which is the same model number as the one in the airplane. The MFD shows the status of both batteries, torque going into each motor, blade pitch angle, and the input level of the torque lever. Additionally, the MFD provides critical electrical system, motor bearing, and motor winding temperature warnings to the pilot, as shown in Fig. 6.

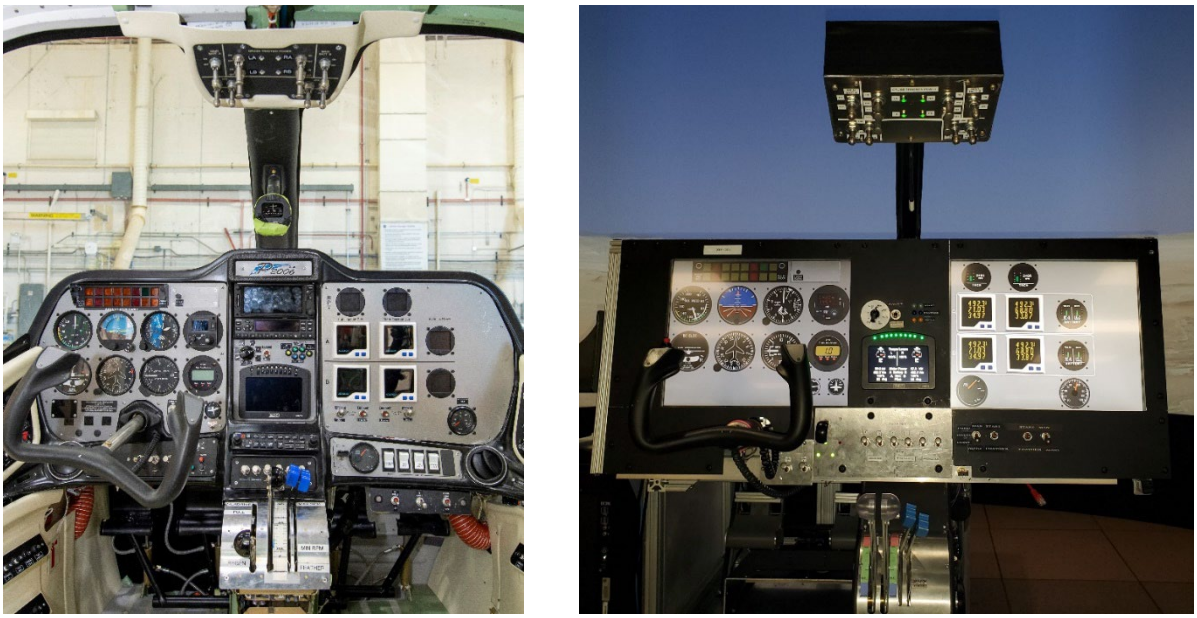

Fig. 4. (left) Aircraft cockpit dashboard; and (right) piloted simulator cockpit dashboard. Photo credit: NASA/Genaro Vavuris.

Audio and visual cautions/warnings of the airplane system are also present in the piloted simulator to provide fault cueing to the pilot. The annunciator panel on the left side of the HDD provides both audio and visual cautions and warnings such as main battery failures, CMC faults, and low voltage. Additional audio and visual annunciations not seen on the annunciator panel but occurring on other locations on the HDD, include propeller hub faults, motor overspeed, and avionics voltage/current out of range.

Mimicking the X-57 airplane, the piloted simulator surface-control inceptors include a yoke that controls the ailerons and elevator along with a rudder pedal assembly which includes toe brakes. Attached to the yoke in the simulator is a force feedback feel system, which produces the predicted forces generated by the aileron and elevator hinge moments. Additionally, for feel familiarity of the yoke, the Mod II right-side yoke of the airplane was repurposed as the simulator yoke.

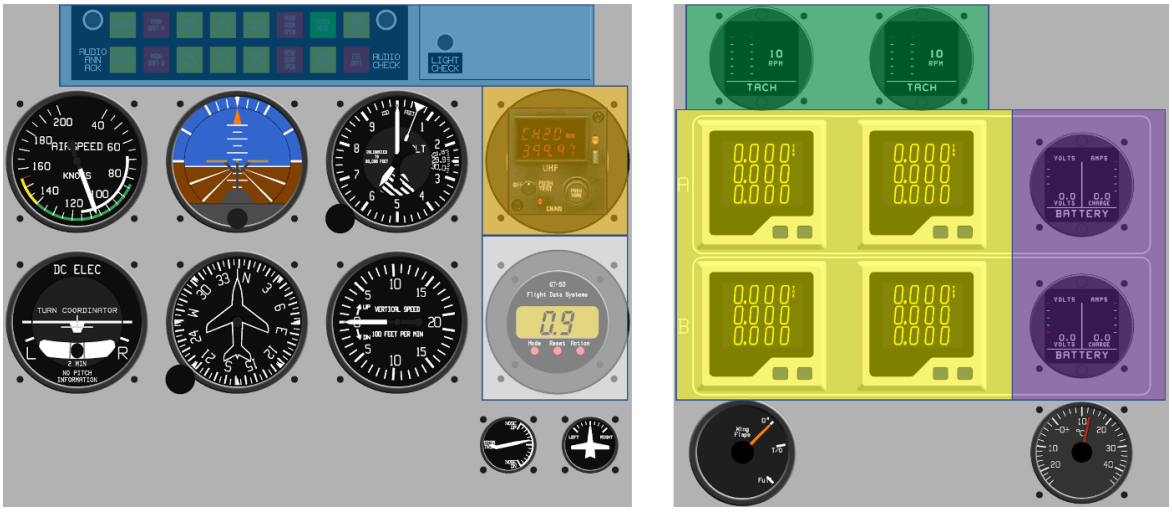

Fig. 5 Head-down display: (left) Panel includes stock P2006T instruments (no shading); radio channel selector (orange shading); annunciator panel (blue shading); and accelerometer (G-meter) (white shading); and (right) panel includes tachometers (green shading); avionic power meters (purple shading); and battery power meters (yellow shading).

For pilot purposes, to emulate the startup and shutdown of the airplane, the critical airplane switches are placed in the simulator cockpit in similar locations as to those on the airplane. The similar placement of the switches is crucial for the pilot in order to memorize switch locations for in-flight emergencies. On the dashboard simulator are the low-voltage switches for the essential bus, DC converters, cross buses, wing avionics, and avionics buses. The high-voltage switches that activate/deactivate the main batteries, cruise traction power, and cruise motor controllers are located on an overhead panel; these are locking switches that match the parts and locations of those on the airplane.

Fig. 6. Multifunction display (MFD); and page selector switches.

Torque motor input and propeller pilot control of the cruise motors are achieved by using two torque levers and two propeller pitch levers, respectively, as shown in Fig. 4. The three distinct regions for torque motor inputs which are separated by lever detents are: regeneration, nominal, and overdrive. For propeller control, the pilot commands a desired RPM using the propeller pitch levers. At the full aft-propeller pitch lever position, a switch commands the propellers to feather.

The simulator cockpit also includes the right seat from the airplane.

IV. Predicted Mod II X-57 Flying Qualities Results

The Mod II piloted simulator was utilized to predict the stability and flying qualities throughout the expected flight envelope. This analysis provides an estimate of the airworthiness of the X-57 airplane as well as the accuracy of the simulator when used as a training and flight-development tool. To examine points throughout the potential operational envelope, three airplane configurations were examined: cruise, takeoff, and landing. For cruise configuration, flaps and landing gear were retracted; for takeoff configuration, flaps were deployed at 15 degrees and landing gear deployed; and for landing configuration, flaps were deployed at 40 degrees and landing gear was deployed.

A. Static Stability

The X-57 project employed Federal Aviation Regulations (FAR) to help give guidance for prediction of the Mod II static stability. For the longitudinal static stability, FAR §23.173 and the corresponding FAR §23.175 [11] were utilized. The FAR §23.173 ensures that the control system friction is not excessive and that the stick force curve versus airspeed is sufficiently steep for safe operations. The FAR §23.175 describes the procedure to determine if the

stick force curve is adequate and if the airplane will free return to trim. The project defined two piloted simulator test maneuvers, based on the conditions and procedure set in the FAR §23.175, to determine if Mod II would meet the requirements. The first maneuver had the pilot trim the airplane then hold a longitudinal displacement into the yoke to capture approximately 10-knots (kts) off the trim and note the yoke force direction and amplitude required to maintain the off-trim condition. After trimming the airplane, the second maneuver had the pilot set a longitudinal yoke displacement, then slowly release the yoke and observe if the airplane returned to within ±10 percent of trim speed. For both maneuvers, the pilots examined various trim speeds with different airplane configurations to ensure airspeed stability throughout the flight envelope.

Two representative flight conditions of piloted simulator data for the first maneuver to maintain an off-trim airspeed with a yoke displacement are shown in Fig. 7 and Fig. 8. In the airplane takeoff configuration, at a trim airspeed of 1.4·Vs1 (84 kts), Fig. 7 shows that for a push of the yoke the airplane speeds up above trim, and the force-feedback system provides a restoring force towards the neutral position. Fig. 8 shows that for a trim airspeed of 1.4·Vs0 (82 kts) in the airplane landing configuration, a push of the yoke will slow the airplane down to below trim, and the force-feedback system provides the opposite direction, restoring force towards the neutral position.

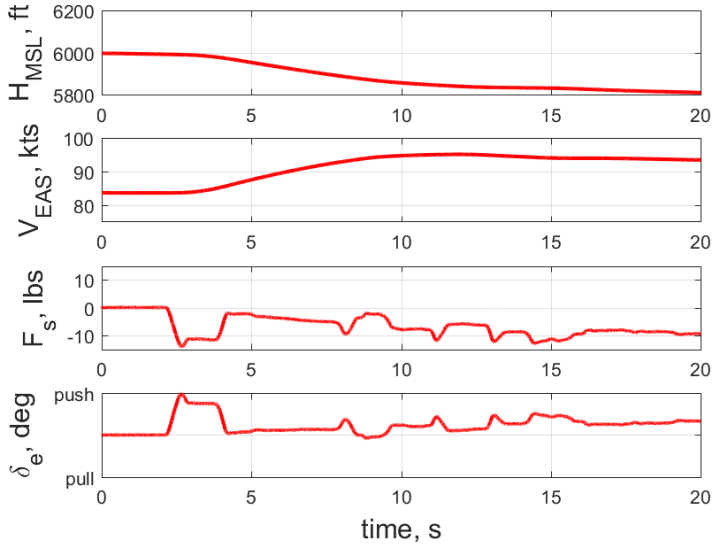

Fig. 7. Piloted simulator time history of a longitudinal yoke push in the takeoff configuration.

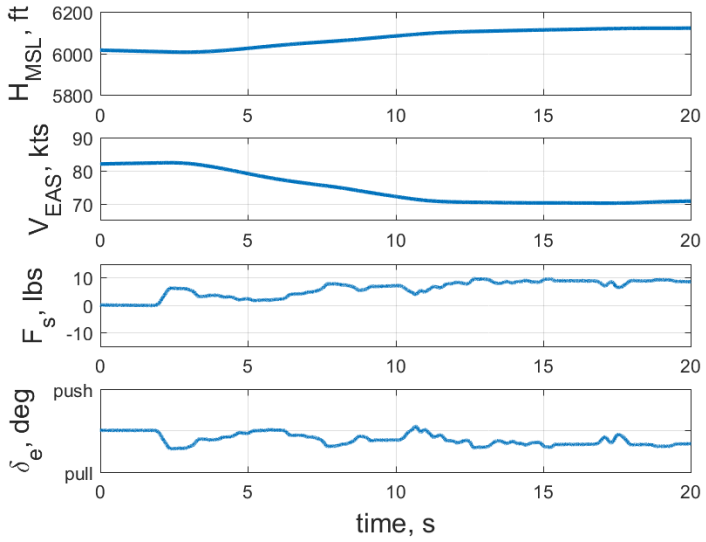

Fig. 8. Piloted simulator time history of a longitudinal yoke pull (in the landing configuration).

Shown in Figs. 9 and 10 is the piloted simulator data for two representative flight conditions of the second maneuver in which the yoke is displaced from trim, then slowly released. Figure 9 shows the airplane takeoff configuration at 1.4·Vs1 (84 kts), after the yoke is released from a push, the airspeed damps out to within ±10 percent of the trim speed in about 30 seconds. As shown in Fig. 10, for a pull followed by a slow release of the yoke (in the airplane landing configuration case), at 1.4·Vs0 (82 kts), the airspeed recovers to below ±10 percent of the trim in about 35 seconds.

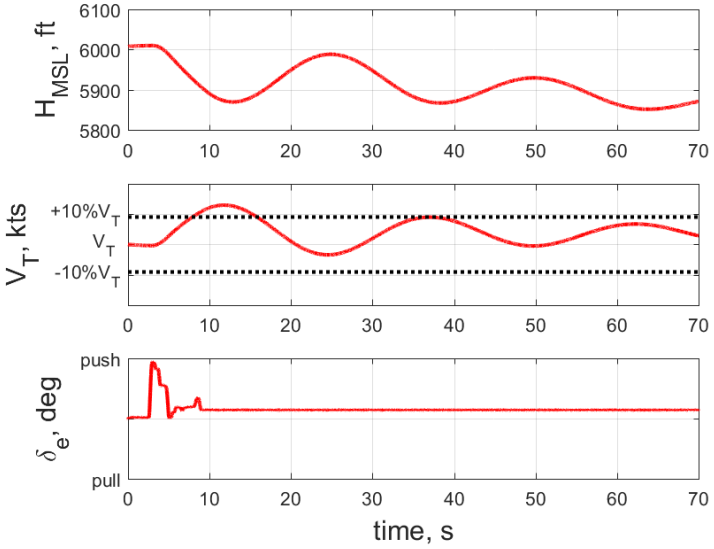

Fig. 9 Piloted simulator time history of a longitudinal yoke perturbation in the takeoff configuration.

.

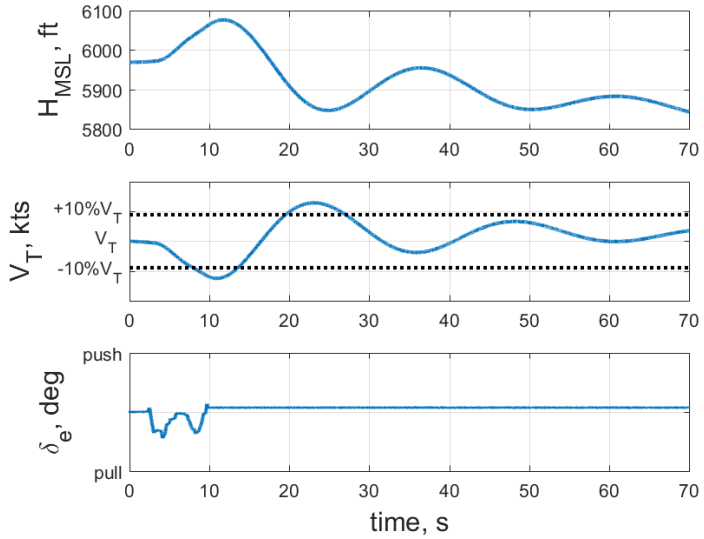

Fig. 10. Piloted simulator time history of a longitudinal yoke perturbation (in the landing configuration).

Longitudinal static stability can also be observed by the relationship between the pitching moment coefficient (C_M) and angle of attack (α). If the slope of the C_M versus α is negative, the airplane is longitudinally static stable [12]. Figure 11 shows that for landing, takeoff, and cruise airplane configurations through a range of α, the C_M curves have negative slopes which correspond to a statically stable airplane.

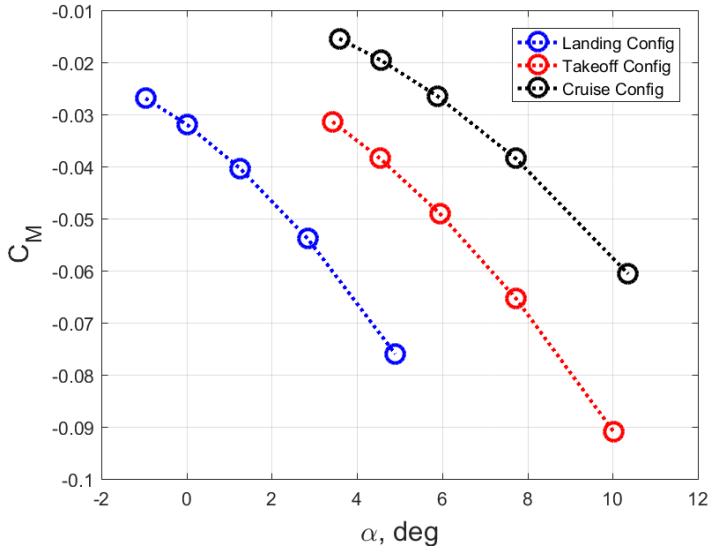

Fig. 11. Pitching moment versus angle of attack for three different airplane configurations.

Longitudinal static stability can also be observed by the relationship of the elevator deflection at trim (δ_e) and lift coefficient (C_L). For subsonic airspeeds, a negative slope of the δ_e and C_L curve will show static stability due to the relationship between C_M, α, and C_L [12]. Examining the elevator trim position at several different C_L values show the predicted longitudinal static stability at various locations in the flight envelope. Although the CG will not be shifting during flight, Fig. 12 shows the predicted elevator trim position at various C_L values at both longitudinal and CG (full forward and full aft of the allowable P2006T) limits. For each of the flap configurations, Fig. 12 shows a negative slope for increasing C_L, which indicates that the airplane is longitudinally static stable throughout the flight envelope. The case of full flaps and full-aft CG still shows a negative slope but has less slope than the other flight configurations, which indicates that at this location the airplane is becoming less stable.

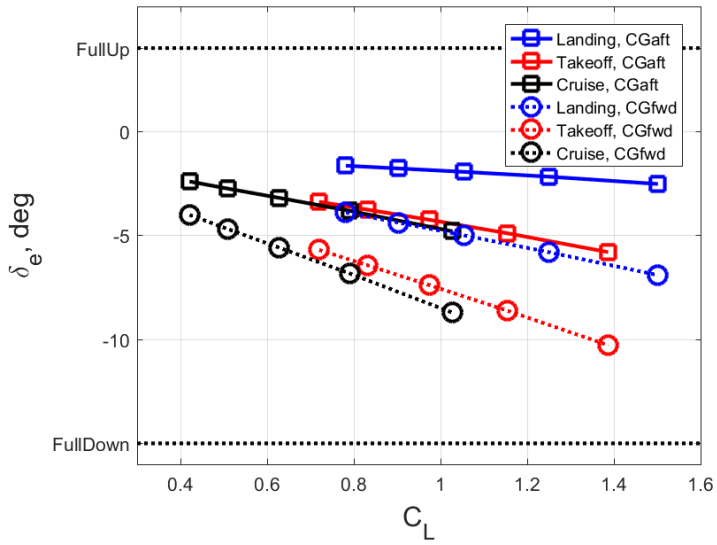

Fig. 12. Simulation analysis of lift coefficient versus elevator trim position for three different airplane configurations and the two Center of Gravity limits.

For lateral static stability guidance, the X-57 project used the FAR §23.177 [11] as guidance to predict lateral static stability of the Mod II airplane in the piloted simulator. The pilot performed a wings-level sideslip maneuver then release of both aileron and rudder controls to observe if the airplane would recover to steady bank and sideslip. This maneuver was performed at two airplane configurations (takeoff and landing) and at multiple trim speeds. As shown in Fig. 13, the sideslip angle (β) and roll angle (Φ) "weathervane" back to a steady lateral position after control release of the right pedal, wings-level sideslip (in the takeoff configurations) at a trim speed of 1.2·Vs1 (72 kts). The landing configurations at a trim speed of 1.2·Vs1 (72 kts), left pedal, wings-level sideslip show that after control release, the β and Φ recover to near trim conditions, as shown in Fig. 14.

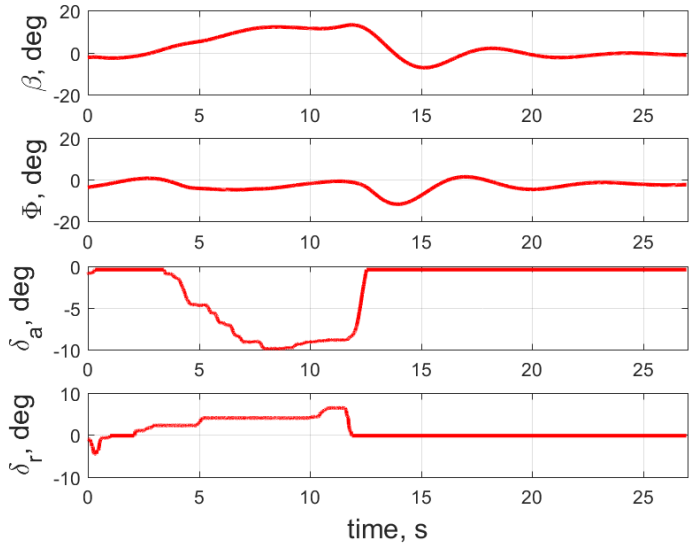

Fig. 13 Piloted simulator time histories for a steady wings-level sideslip maneuver (in the takeoff configuration).

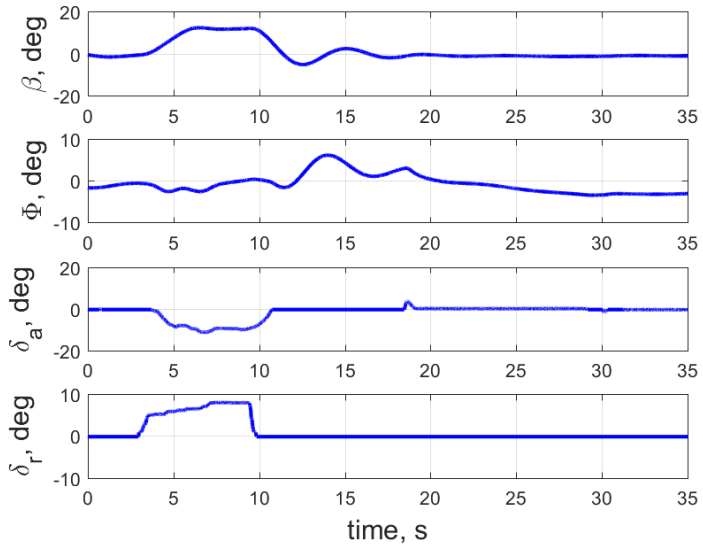

Fig. 14 Piloted simulator time histories for a wings-level sideslip maneuver (in the landing configuration).

A lateral static stability simulation study, shown in Fig. 15, was performed to examine the required rudder (δr) and aileron (δa) deflections needed to maintain trim in a wings-level sideslip. A negative rudder input, (left pedal) requires a positive aileron input (right yoke); and a positive rudder input (right pedal) requires a negative aileron input (left yoke) [12]. The results clearly show that the airplane has lateral static stability by having the expected inputs to maintain a wings-level sideslip.

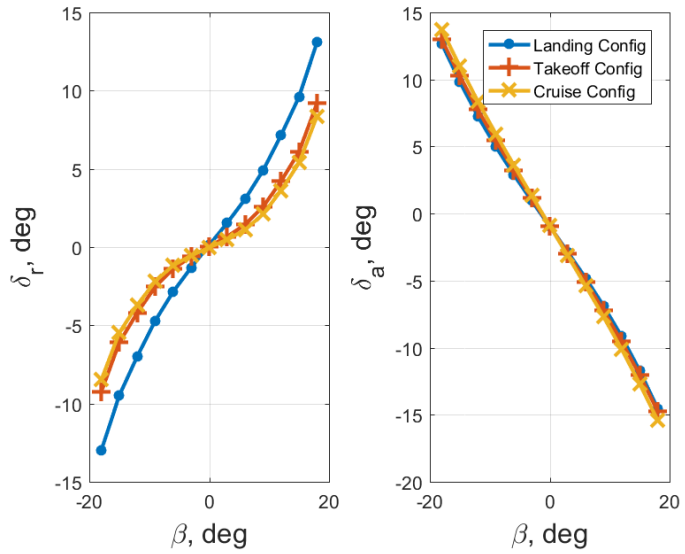

Fig. 15 (left) Simulation analysis of sideslip angle versus rudder position; and (right) sideslip angle versus aileron position.

B. Linear Modal Analysis and Handling Qualities Predictions

To predict the dynamic stability throughout the Mod II flight envelope, the X-57 piloted simulator was used to obtain state-space models at various flight conditions and airplane configurations. Linearized models were taken at the following configurations: landing (from 58 to 81 kts); takeoff (from 60 to 84 kts); and cruise (from 90 to 130 kts). The predicted phugoid, short period, roll, and Dutch roll mode requirements from the military standards handbook, MIL-STD-1797B [13] were used for the flying qualities of the Mod II X-57 assessments.

Phugoid Mode

The phugoid mode, which is characterized as a low-frequency longitudinal oscillation, is considered a nuisance motion that the pilot can easily control. The eigenvalues of the state space models related to the phugoid mode are shown in Fig. 16. Since the locations of the predicted phugoid mode (shown in Fig. 16) are in the negative position of the real axis (Real Eig) and are nonzero for the imaginary axis (Imag Eig), mode is, therefore, shown to be stable throughout the flight envelope. In addition, Fig. 17 shows that utilizing the MIL-STD-1797B requirement for phugoid damping produces Level 1 flying qualities for the phugoid mode. Fig. 17 also shows, for each airplane configuration, as the speed increases the phugoid mode damping also increases.

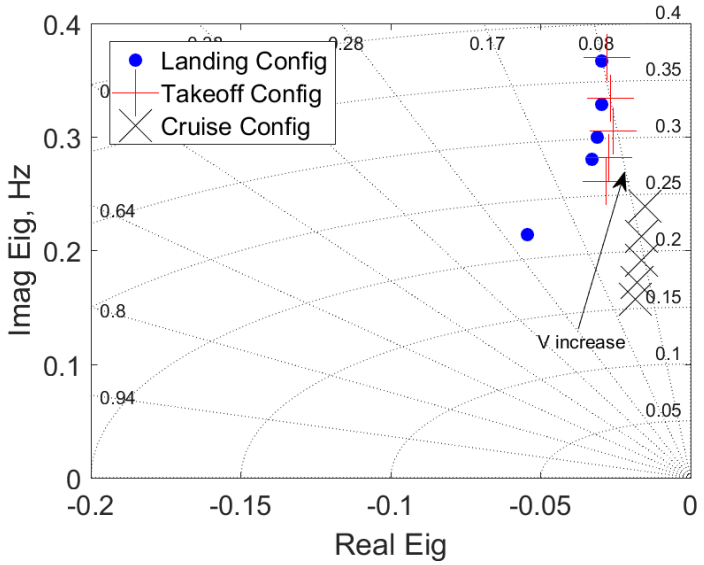

Fig. 16 Phugoid eigenvalues of the state space models at various locations in the flight envelope.

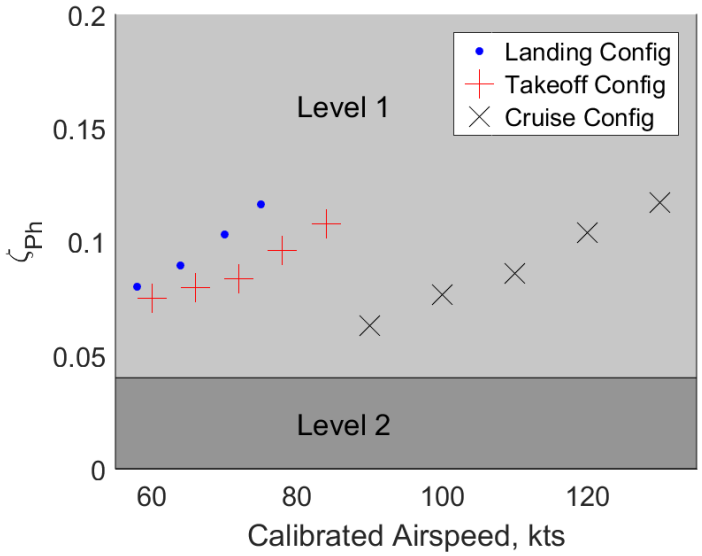

Fig. 17 Phugoid damping versus airspeed.

Short Period

Prediction of the dynamic stability of the higher frequency, longitudinal oscillation short-period mode is represented by the eigenvalues of the linearized model, as shown in Fig. 18. By examining the real and imaginary

eigenvalue parts of the state-space models for each of various points in the flight envelope, a stable short period is shown.

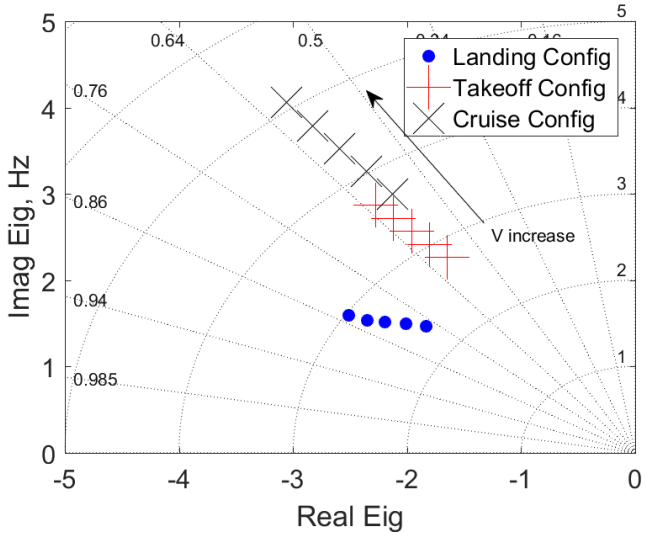

Fig. 18 Short-period mode eigenvalues of the state-space models at various locations in the flight envelope.

Using the short-period mode, the flying qualities MIL-STD-1797B requirement for the takeoff/landing flight phase (Cat C), Fig. 19, shows the simulation predicted results of the control anticipation parameter (CAP) versus short-period damping in the top panel as well as short-period damping versus airspeed in the bottom panel. According to the MIL-STD-1797B, the CAP is the ratio of initial pitching acceleration to normal acceleration, as defined in Eq. (3), which relates to the aircraft longitudinal response sensitivity to a pitch command.

$$CAP = \frac{\omega_{sp}^2}{n/\alpha} = \frac{\omega_{sp}^2}{\frac{V}{g}\frac{1}{T}} \tag{3}$$

Throughout the flight envelope, the top panel of Fig. 19 shows that the anticipated CAP has Level 1 flying qualities for the expected airplane short-period damping. Also shown, for each airplane configuration in the top panel, as the short-period damping increases, the frequency decreases. Level 1 flying qualities for the predicted short-period damping across various airspeeds are shown in the bottom panel of Fig. 19. As the airspeed increases in the bottom panel, there is a slight increase in damping for each airplane configuration.

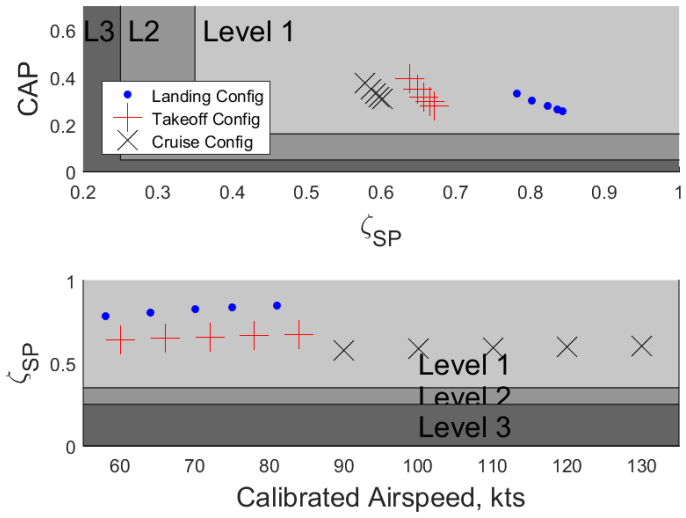

Fig. 19 (top) The control anticipation parameter versus short-period damping; and (bottom) short-period damping versus airspeed.

Roll Time Constant

Evaluation of the dynamic lateral-directional stability for the non-oscillatory roll mode looks at the roll time constant (τ_r). The roll time constant relates to the response of the airplane to an aileron step input and indicates the quickness of the airplane to develop a steady roll rate. For each airplane configuration, the roll time constant is predicted to decrease as the airspeed increases, as shown in Fig. 20. In the Mod II flight envelope, Fig. 20 shows that the expected roll time constants will be within Level 1 flying qualities, per MIL-STD-1797B requirements.

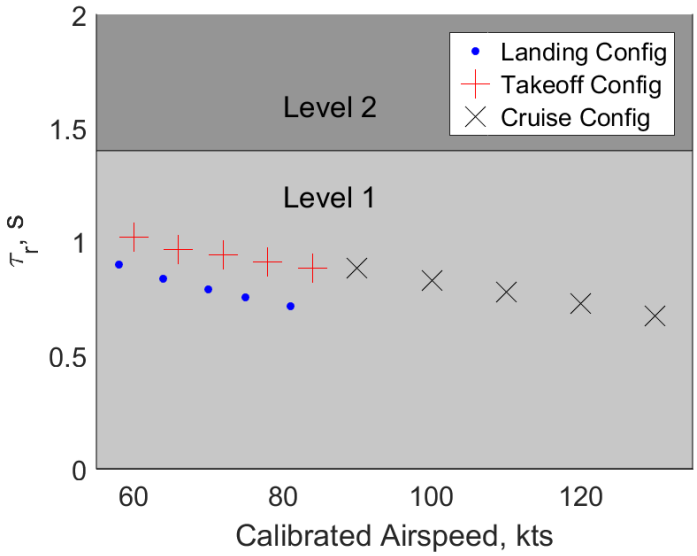

Fig. 20 Roll mode, roll mode time constant versus airspeed.

Dutch Roll

The lateral, oscillatory Dutch roll mode dynamic stability was evaluated by assessing the eigenvalues of the state-space models as seen in Fig. 21. The real part of the eigenvalues are negative and imaginary parts are nonzero; thus, indicating that the airplane will have a stable Dutch roll mode.

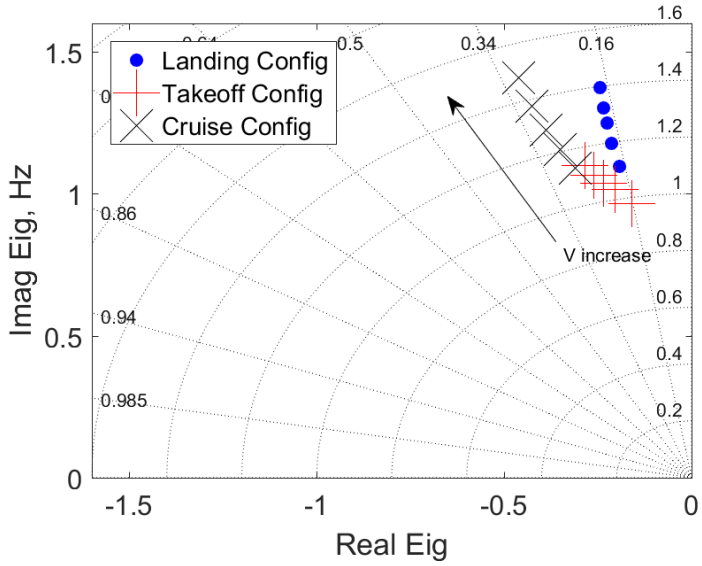

Fig. 21 Dutch roll eigenvalues of the state-space models at various locations in the flight envelope.

In addition to assessing the eigenvalues of the state-space models, the Dutch roll mode MIL-STD-1797B damping requirements were employed to predict the flying quality levels throughout the flight envelope. As seen in Fig. 22, the predicted Dutch roll damping shows Level 1 at various airplane configurations and airspeeds. In Fig. 22, as the airspeed increases for both flaps in the cruise and takeoff configurations, the Dutch roll damping increases, while for flaps in the landing configuration, the damping levels off above 64 knots.

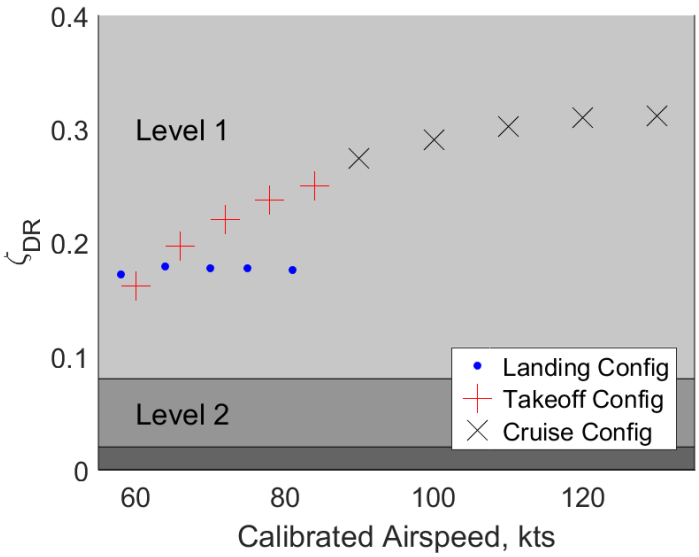

Fig. 22 Dutch roll mode, damping versus airspeed.

V. Conclusion

A pilot-in-the-loop, fixed-base non-linear simulator has been developed for the Mod II X-57 "Maxwell" airplane.

The piloted simulator included models of the aerodynamics, propulsion, mass properties, landing gear, and electrical system of the airplane and were developed and integrated into a simulator to replicate the Mod II. In addition

to the integrated models, a realistic cockpit was built which encompassed pilot inceptors, propulsion effectors, electrical switches, digital dashboard gauges, audio warnings, and a (CAN) messaging display.

Stability and flying quality prediction studies were conducted using the simulator. The pilots performed longitudinal and lateral directional maneuvers and demonstrated that the airplane should be statically stable in both axes. Simulation analysis of lift coefficient versus elevator deflection, and sideslip angle versus lateral control also indicates that the airplane will have static stability. Dynamic stability was also exhibited by linearizing the simulator at various points throughout the expected flight envelope and evaluating the eigenvalues of the longitudinal and lateral modes. Using the linearized simulation data, it is predicted that phugoid, short period, roll-time constant, and the Dutch roll mode will have Level 1 flying qualities, based on the MIL-STD-1797B requirements. The integrated models and replicated cockpit of the Mod II X-57 piloted simulator provided a platform for pilot training, mission rehearsals, and evaluation and prediction of the flight dynamics of the airplane. The batch and pilot-in-the-loop simulator analysis will predict whether the airplane will be stable with Level 1 flying qualities throughout the flight envelope.

VI. Planned Future Work

After the Mod II airplane has successfully flown, the data from the flights will be compared to the predictions from the simulator to evaluate the accuracy of the simulation results.

References

[1] Moore, M. D., and Fredericks, B., "Misconceptions of Electric Aircraft and their Emergent Aviation Markets," AIAA Paper 2014-0535, January 2014. doi.org/10.2514/6.2014-0535.

[2] Borer, N. K., Patterson, M. D., Viken, J. K., Moore, M. D., Clarke, S., Redifer, M. E., Christie, R. J., Stoll, A. M., Dubois, A., Bevirt, J., Gibson, A. R., et al., "Design and Performance of the NASA SCEPTOR Distributed Electric Propulsion Flight Demonstrator," AIAA Paper 2016-3920, June 2016. doi.org/10.2514/6.2016-3920.

[3] Clarke, S., Redifer, M., Papathakis, K., Samuel, A., and Foster, T., "X-57 Power and Command System Design," 2017 IEEE Transportation Electrification Conference and Expo (ITEC), 2017, pp. 393-400. doi.org/10.1109/ITEC.2017.7993303.

[4] Costruzione Aeronautiche Tecnam srl, "P2006T - Aircraft Flight Manual," Doc. No. 2006/044 3rd ed., Rev. 4, Capua, Italy, May 2014.

[5] Mathworks, Inc., MATLAB and Simulink, Software Package, Version 2016b, Natick, MA, https://mathworks.com [retrieved June 2020].

[6] Castro, M, "AFRC Core Simulation Overview," NASA Doc ID. 20150007885. April 2015. https://ntrs.nasa.gov/search?q=AFRC%20Core%20Simulation%20Overview [retrieved 19 April 2023].

[7] Nicolosi, F., De Marco, A., and Vecchia, P.D., "Stability, Flying Qualities and Parameter Estimation of a Twin-Engine CS-23/FAR 23 Certified Light Aircraft," AIAA Paper 2010-7947, August 2010. doi.org/10.2514/6.2010-7947.

[8] MT Propeller, "MT-Propeller Operation and Installation Manual,", Doc No. E-118, ATA 61-01-18, Revision 40, September 2014.

[9] Drela, M., Massachusetts Institute of Technology, Cambridge, Massachusetts, XROTOR, Software Package.

[10] Chin, J. C., Schnulo, S. L., Miller, T. B., Prokopius, K., and Gray, J., "Battery Performance Modeling on Maxwell X-57," AIAA Paper 2019-0784, January 2019. doi.org/10.2514/6.2019-0784.

[11] Federal Aviation Administration (FAA), "Title 14–Aeronautics and Space," *Code of Federal Regulations*, Parts 1 to 59, 14CFR/Part 23, 2008, pp. 174–350, https://www.govinfo.gov/content/pkg/CFR-2019-title14-vol1/pdf/CFR-2019-title14-vol1.pdf [retrieved 13 April 2023].

[12] Yechout, Thomas R., Morris, Steven L., Bossert, David E., Hallgren, Wayne F., and Hall, James K., *Introduction to Aircraft Flight Mechanics—Performance, Static Stability, Dynamic Stability, and Classical Feedback Control*, Reston, Va., American Institute of Aeronautics and Astronautics, Inc., January 2003. doi.org/10.2514/4.102547.

[13] Department of Defense Interface Standard "Flying Qualities of Piloted Aircraft," MIL-STD-1797, Rev. B, February15, 2006, (Distribution Statement D).